Revealing the Evolution of the Tumor Immune Microenvironment in Follicular Lymphoma Patients Progressing Within 24 Months Using Single-cell Imaging Mass Cytometry

Long Liu
The First Affiliated Hospital of Xiamen University, Xiamen University
Xingxing Yu
The First Affiliated Hospital of Xiamen University, Xiamen University
Zhifeng Li
The First Affiliated Hospital of Xiamen University, Xiamen University
Xiaohua He
Sun Yat-sen University Cancer Center
Jie Zha
The First Affiliated Hospital of Xiamen University, Xiamen University
Zhijuan Lin
The First Affiliated Hospital of Xiamen University, Xiamen University
Yan Hong
The First Affiliated Hospital of Xiamen University, Xiamen University
Huijian Zheng
The First Affiliated Hospital of Xiamen University, Xiamen University
Qian Lai
The First Affiliated Hospital of Xiamen University, Xiamen University
Kaiyang Ding
The First Affiliated Hospital of USTC Anhui Provincial Hospital
Xian Jia
The First Affiliated Hospital of USTC Anhui Provincial Hospital
Guo Fu
Xiamen University
Haifeng Yu
Cancer Hospital of the University of Chinese Academy of Sciences, Zhejiang Cancer Hospital
Haiyan Yang
Cancer Hospital of the University of Chinese Academy of Sciences, Zhejiang Cancer Hospital
Zhiming Li
Sun Yat-sen University Cancer Center

Ken H. Young
Duke University Medical Center
Bing Xu (xubingzhangjian@126.com)
The First Affiliated Hospital of Xiamen University, Xiamen University

---

Research Article

Keywords: FL, TIME, POD, Immune signature, T-cell

Posted Date: April 11th, 2022

DOI: https://doi.org/10.21203/rs.3.rs-1524378/v1

Abstract

Background: The tumor immune microenvironment (TIME) is crucial for follicular lymphoma (FL) pathogenesis and progression. However, TIME evolution during progression of disease within 24 months (POD24) is unknown.

Methods: Spatially-resolved and single-cell image mass cytometry with a panel of 36 meta-tagged antibodies was quantitatively used to dissect the TIME structure in 13 paired FLs at diagnosis and POD24.

Results: Increased $CD163^{-}$ macrophages with PD-1 ligand upregulation and decreased $CD8^{+}$T cells with upregulated LAG3 expression were observed in the follicles during POD24. Spatial interactions demonstrated that FL cells interacted more intimately with macrophages rather than Tregs and less with cytotoxic cells during POD24. Additionally, more $CD8^{+}$T cells near FL cells interacted with macrophages but not Tregs during POD24. Notably, macrophages also cooperated with Tregs more frequently to simultaneously hijack the cytotoxic T-cells and protect FL cells, subsequently generating a more immunosuppressive environment in the follicles during POD24.

Conclusions: FL cells reside in a more immune-compromised microenvironment, evading immune-cell attacks during POD24. Novel immunotherapeutic approaches harnessing LAG3, macrophages, and Tregs will be promising to overcome the poor outcomes of patients with FL POD24.

Background

Follicular lymphoma (FL) is the most common indolent B-cell lymphoma and is generally characterized by the malignant transformation of follicular center B cells harboring the t(14;18) translocation involving the *IgH/bcl-2* genes[1]. Although emerging therapeutic approaches can improve the overall survival (OS), which might even extend beyond 18 years, FL remains an incurable disease with a prolonged, relapsing-remitting course[2]. Notably, patients experiencing disease progression within 24 months of diagnosis (POD24) display an aggressive course and markedly poorer prognosis with an OS of less than 50% after 5 years[3]. However, POD24 biology remains unclear, contributing to a dilemma in developing novel therapeutic approaches to improve clinical outcomes.

FL is considered an immunologically functional tumor and therefore prompts the application of immune-modulating regimens such as lenalidomide or immune checkpoint inhibitors combined with rituximab[1, 4, 5]. Moreover, abundant immune cells in the tumor immune microenvironment (TIME), such as macrophages (Mφs) and regulatory T (Treg), $CD8^{+}$T, and $CD4^{+}$T cells, have reportedly been associated with the progression-free survival of FL patients in the rituximab and pre-rituximab era. Recently, Joshua et al. demonstrated that PD-L2 expression could reflect immune infiltration in the TIME of FL. Patients with high immune infiltration mainly have higher levels of programmed cell death 1 ligands ($PD\text{-}L1^{+}$) macrophages and clonal T cells[6, 7]. Importantly, POD24 in FL has been associated with reduced intra-

tumoral immune infiltration at diagnosis in both discovery and validation cohorts. Consequently, these data indicate that the TIME might play a key role during POD24 in FL. Although the causal association between the TIME at diagnosis and the incidence of POD24 has been well established, the precise features of the TIME at POD24 and the evolution of TIME during POD24 are unknown.

The TIME of FL is composed of various cells, including immune cells such as tumor-infiltrating $CD8^+$T cells, Tregs, Mφs, follicular helper T cells (Tfhs), conventional $CD4^+$T cells (Tcons), follicular dendritic cells (FDCs), and structural cells, such as fibrotic reticular cells (FRCs) and endothelial cells[4, 8]. A comprehensive exploration of TIME evolution during POD24 would not only cover dynamic alterations in the number of cell types but would also include the cell states and cell–cell interactions, which is ultimately essential for designing strategies to prevent POD24 in FL. Therefore, applying technologies that enable a comprehensive spatial analysis at single-cell resolution with high-throughput phenotypic information is critical for fully revealing the TIME. Recently, highly multiplexed tissue imaging technologies based on cyclic immunofluorescence or epitope-targeted mass spectrometry and RNA detection have emerged and could be useful to comprehensively review marker distribution and tissue composition[9, 10].

Imaging mass cytometry (IMC) uses laser ablation on tissues at a resolution of 1 μm to generate plumes of particles that are carried to and analyzed by mass cytometry. IMC enables the simultaneous evaluation of up to 50 biomarkers from tissue sections stained with metal-tagged antibodies[11–15]. Using IMC data, a pathognomonic map of TIME heterogeneity was established, revealing the evolution of cell compositions and interactions between FL and immune cells, and providing a fundamental basis for novel therapeutic strategies to overcome the poor outcomes of patients with FL POD24.

Methods

Patient characteristics and sample preparation

In total, 39 paraffin-embedded lymph node samples from FL patients, including 26 samples at diagnosis and 13 paired samples at POD24 from the First Affiliated Hospital of Xiamen University and Sun Yat-sen University Cancer Center from September 2001 to September 2018, were enrolled in this study. The patient characteristics are summarized (supplementary table 1). Briefly, the median patient age was 57 years. Half of the patients were diagnosed with grades 1–2, and 42% (11/26) and 8% (2/26) were diagnosed with grades 3A and 3B disease, respectively. Most patients (24/26) received rituximab-based immunochemotherapy, except for two patients who underwent chemotherapy. After frontline therapy, 73% of patients achieved complete remission (CR), whereas 23% (6/26) achieved partial remission, and one patient remained stable. For patients with POD24, the median time to progression was 562 days. In total, 38% (5/13) failed to achieve CR after first-line therapy.

All tissue sections were produced to a thickness of 5 μm. Regions of interest (ROIs) covering the follicular and interfollicular areas were selected according to the locations of consecutive sections stained with

hematoxylin-eosin. For patients with disease that transformed into diffuse large B-cell lymphoma, ROIs covering malignant follicles were selected according to CD21 and Bcl-2 expression in the germinal center. All samples were obtained after the patients provided informed consent. IRB approval for this study was granted by the Institutional Human Ethics Review Committee of the First Affiliated Hospital of Xiamen University and Sun Yat-sen University Cancer Center, in accordance with the Declaration of Helsinki.

Antibody conjugation and staining

For antibodies without available conjugated metal in Fluidigm, conjugated metal and primary antibodies were constructed as described previously[16]. Following conjugation, the antibodies were diluted in 0.5% BSA and stored at 4°C for staining. Slide-tissue sections were baked at 67 °C for 30 min. Tissue sections were deparaffinized with two washes of 100% fresh-xylene and then rehydrated with successive washes with ethanol 100% (2×), 95% (2×), 85% (1×), 70% (1×), and distilled water. The sections were then immersed in antigen retrieval buffer (tris-EDTA buffer, pH 9.0; Abcam, Cambridge, UK), incubated at 97 °C for 30 min, and cooled to room temperature at room temperature. Slides were washed with distilled water (1×) and Dulbecco's phosphate-buffered saline (1×) for 10 min each and then washed with distilled water for 8 min on an orbital shaker. Next, the tissue was blocked with blocking buffer for 30 min at 25–30°C (Superblock Blocking Buffer in PBS; Thermo Fisher Scientific, Waltham, MA, USA) in a humid chamber. After blocking, the antibody mix was then applied with the dilutions indicated in supplementary table 2 and incubated overnight at 4 °C in a humid chamber. After overnight incubation, the slides were washed on an orbital shaker for 5 min in wash buffer. Thereafter, tissue sections were successively washed with 0.2% triton X-100 (2×) and D-PBS (2×) on an orbital shaker. Subsequently, slides were incubated with intercalator-Ir diluted 1:400 in D-PBS for 30 min at room temperature. After incubation, the sections were washed with distilled water for 5 min. Finally, the slides were dried under airflow for 5 min and stored at 4 °C until ablation.

IMC acquisition

The Hyperion mass cytometry system (Fluidigm Corporation, South San Francisco, CA, USA) was autotuned using a 3-element tuning slide according to the tuning protocol provided by the manufacturer. As an extra threshold for successful tuning, a detection of at least 1,500 mean duals of 175 Lu was used. ROIs were selected based on consecutive tissue sections stained with hematoxylin and eosin. ROIs of 1,000 × 1,000 μm were ablated and acquired at 200 Hz for approximately 2 h. Data were exported as MCD files and visualized using the Fluidigm MCD™ viewer. To better separate the antibody signal and noise, each marker was visually inspected, and a minimum signal threshold of one or two dual counts was set in the Fluidigm MCD™ viewer.

Cell segmentation

For cell segmentation of non-immune cells, we employed DNA-Iridium staining as nuclear and cell membrane markers to define primary and secondary objects. CellProfiler was subsequently used to define the cell masks and quantify marker expression. To define cell borders, nuclei were first identified as

primary objects based on ilastik probability maps and expanded through the cytoplasm compartment until either a neighboring cell or the background compartment was reached. Next, cell masks were generated to identify single cells and used to extract single-cell information (marker abundance, spatial, and neighborhood data) from the original images. Finally, the results were exported as .tiff for analysis.

Image visualization and phenotypic analysis

Each sample and mask were imported into HistoCAT version 1.76[17], and the intra- and inter-follicle regions were gated according to CD19 and SMA expression. After gating, each lymph node sample that was noted to morphologically span both the outer and inner stripes was exported from HistoCAT as a csv file, including the cell ID, signal strength of markers, and coordinates of each cell. Data were analyzed and graphed using R and HistoCAT software. the R implementation of FlowSOM (https://github.com/SofieVG/FlowSOM) was used to define the cell type. In particular, an R implementation of tSNE (https://cran.r-project.org/web/packages/tsne) was used to generate tSNE maps. Log_{10} transformation was applied as indicated in the figures. Unless otherwise stated, the raw IMC counts were 99th-percentile-normalized and scaled from 0 to 1 (scaled counts)[18].

Neighborhood and cell interaction analysis

Neighborhood analysis was performed using R and HistoCAT software. Custom scripts were used to import the cell type into HistoCAT. An expansion of four pixels from the center of cells was used to detect the cell neighbors[17]. Interaction pattern analysis for Tregs, Mφs, $CD8^+$T cells, and FL cells was performed as follows. A unique ID was assigned to each identified cell. The IDs of all cells surrounding a cell could be extracted in a csv file via HistoCAT. Based on the cellular phenotypes, cells were classified into different cell types including Tregs, Mφs, CD8+T cells, and FL cells. We analyzed the interactions of each cell type with the other three cell types and further categorized the cells into eight groups according to the interaction patterns of four general interaction patterns as follows: simultaneous interaction with other three cell types, interaction with any two of three other cell types, interaction with only one of three other cell types, and no interactions with any other cell types (as shown in Figure 5A, 6A, 7A). The number of cells in each pattern could be calculated according to the cell IDs. All other parameters and methods were chosen as suggested in the original publication[17].

Statistical analysis

Statistical tests were performed using R. The statistical parameters are reported in the figure legends. For pairwise group comparisons, we used a non-parametric statistical test (an unpaired two-tailed Mann–Whitney *U* test). Overall, the *p*-value significance threshold was set at 0.05.

Results

Image data acquisition and processing of FL tissues using IMC

In total, 39 lymph node samples from FL patients, including 26 FL samples at diagnosis and 13 paired samples at POD24, were subjected to IMC analysis after staining with 36 meta-tagged antibodies (Fig. 1A). As shown in Figure 1, the overlay of selected markers enabled the visualization of immune components, such as FL cell staining for CD19 and Bcl-2 in follicles (normal germinal center B cells do not express Bcl-2; Fig. 1B–D), $CD4^+$ and $CD8^+$ T cells (Fig. 1E, F), macrophages (CD68, Fig.1G), and structural cells such as FDCs (CD21, Fig. 1I) and FRCs (SMA and vimentin, Fig. 1I). In addition, the interfollicular region and follicles could be precisely gated using SMA, vimentin, and CD21 (Fig. 1I). After cell segmentation (Fig. 1J), spatial and phenotypic data were extracted and subjected to analysis of cell categories (Fig. 1K), marker expression (Fig. 1L), neighborhood relationships, and cell–cell interactions (Fig. 1M).

Landscape of the TIME in FL as revealed by IMC

To further illustrate the landscape of the TIME, the cell components were classified by their canonical marker expression. In total, 12 clusters in the tumor environment were displayed, including four FL subsets (clusters 1, 8, 10, and 11); two subsets of $CD4^+$ helper T cells (Th) distinguished by inducible T-cell costimulator (ICOS) expression including cluster 2 ($ICOS^-$Th) and cluster 12 ($ICOS^+$Th); two types of tumor-associated Mφs (TAMs), including cluster 4 ($CD163^+$Mφs) and cluster 6 ($CD163^-$Mφs); $CD8^+$ T cells (cluster 5); normal B cells (cluster 9); and Tregs (cluster 7) in the TIME (Fig. 2A). We further quantified clusters in the follicular and interfollicular regions. As a result, TAMs, $ICOS^-$Th (cluster 2) and $CD8^+$T cells as well as FRCs were significantly increased in the interfollicular regions, whereas four FL subsets, normal B cells and $ICOS^+$Th (cluster 12) were more abundant in follicles (Fig. 2B, C). Consequently, cellular compositions in immune microenvironments of FL showed heterogeneities in spatial distribution that could be comprehensively revealed by IMC.

Evolution of immune and tumor compositions in the follicular and interfollicular area during POD24 in FL

Although immune compositions in the TIME at diagnosis were reported to be associated with POD24 in FL, the evolution of immune cells and its mechanisms in the TIME during POD24 are unknown. As cellular compositions were highly heterogeneous in the intra- and inter-follicle regions, we separately evaluated the dynamic alterations in inter- and intra-follicular region immune components during POD24 in FL. In the follicles, we found that the frequency of $CD163^-$Mφs (cluster 6) was significantly higher at POD24 (Fig. 3A, C). However, unlike that in the follicular regions, the percentage of $CD163^+$Mφs, rather than $CD163^-$Mφs, in the interfollicular regions was markedly elevated at POD24 (Fig. 3B). In addition to that of $CD163^+$ Mφs, the frequency of interfollicular $ICOS^-$Th was significantly decreased after POD24 (Fig. 3B). Additionally, regarding FL cells, only the percentages of cluster 8 ($CD27^+CD45RO^-HLA\text{-}DR^+$) in the interfollicular regions were significantly decreased at POD24, whereas FL subsets in the follicles were not significantly altered (Fig. 3B). Further phenotypic analysis showed higher expression of programmed cell death protein ligand 1(PD-L1) rather than PD-L2 in FL cells (cluster 8) in the interfollicular area after

POD24 (Fig. 3D). Thus, TAMs evolved distinctly in the follicular and interfollicular areas along with a few other subsets, including Tcons and cluster 8.

Imbalanced evolution in TAMs and $CD8^+$ T cells surrounding FL cells results in a more immunosuppressive TIME in follicles after POD24 in FL

Although immune and most tumor cells reside in the follicles, they do not accurately represent the neighbors of FL-cells owing to the existence of other components in the follicles, such as normal B cells and FRCs or FDCs. Therefore, we evaluated the evolution of the immune cells neighboring FL-cells at POD24 according to their location information. Consistent with the total follicle data, the percentage of $CD163^-$Mφs in the vicinity of FL-cells was significantly increased after POD24, whereas $CD8^+$ T cells around FL cells showed a significant decrease (Fig. 4A). Further phenotypic analysis showed that $CD163^-$Mφs around FL cells displayed higher expression of PD-L1 and PD-L2 after POD24 (Fig. 4C). Regarding $CD8^+$T cells neighboring FL cells, higher expression of lymphocyte-activation gene 3 (LAG3), but not programmed cell death protein 1(PD-1), was observed in the POD24 group (Fig. 4B). These data suggest that immune cells in follicles are involved in the POD24 of FL; notably, an increase of $CD163^-$Mφs with upregulation of PD-1 ligands, and a decrease in cytotoxic $CD8^+$T cells, but with upregulated expression of immune checkpoints, might facilitate the formation of an immunosuppressive microenvironment during POD24 in FL.

Dynamic changes in interactions between tumor and immune cells during POD24 in FL

Microenvironments presented at POD24 in FL were found to have evolved to be more immunosuppressive, as mentioned previously herein. Cytotoxic T cells were considered the main effector cells that kill FL cells, whereas Treg and TAMs were the main immunosuppressive cells restricting $CD8^+$T cell functions in the TIME. Tumor cells that interact with different immune cells could represent different immune response statuses. We classified FL cells according to the co-localization patterns with Mφs, Tregs, and $CD8^+$T cells, as shown in Fig. 5A. Eight interaction patterns between FL cells and the three types of immune cells were described, and the percentages of FL cells with different interaction patterns accounting for total FL cells were calculated (Fig. 5A). As a result, we found that the proportion of FL cells interacting with $CD8^+$T cells alone (pattern 2) was significantly reduced in follicles after POD24 (Fig. 5B). However, FL cells interacting with Mφs alone (patterns 4) and simultaneously with and Tregs (Pattern 7) were robustly increased in follicles after POD24 (Fig. 5C, D). Similarly, a significant decrease in FL cells interacting with $CD8^+$T cells alone (pattern 2) and an increase in FL cells interacting with Mφs alone (pattern 4) were observed in the interfollicular regions after POD24 (Fig. 5E, F). These data suggest that more FL cells are protected from immune attack via spatial distancing from cytotoxic T cells and interacting immunosuppressive cells, and especially Mφs.

More frequent cooperation between TAMs and Tregs in hijacking cytotoxic T cells contributes to TIME evolution into enhanced immune-escaping potential during POD24 in FL

Although $CD8^+$T cells contributed to the predominant cytotoxic effects on tumor cells, their cytotoxic function was generally suppressed by regulatory cells such as Tregs and TAMs. However, whether Tregs and TAMs suppressed $CD8^+$T cells separately or cooperatively in the TIME of FL and how the interaction pattern evolves during POD24 remained unknown. To explore the immunosuppressive pattern of TAMs and Tregs, we analyzed the fractions of Tregs around TAMs, accounting for total Tregs (Fig. 6A). As a result, a larger fraction of Tregs around Mφs was observed after POD24 (Fig. 6B). An analysis of the interaction patterns among Tregs revealed that more Tregs cooperated with Mφs after POD24 in a manner similar to that of Patterns 4 and 7 (Fig. 6C, D), but the frequency of Tregs inhibiting $CD8^+$T cells near FL cells alone (Pattern 5) was significantly decreased (Fig. 6E), indicating that Tregs evolved to serve their regulatory function by cooperating more frequently with Mφs, rather than by themselves, after POD24. $CD8^+$T cells are the main targets of Tregs and Mφs. Therefore, we similarly classified $CD8^+$T cells according to their interaction patterns, as mentioned previously herein (Fig. 7A). Consistently, more $CD8^+$T cells were hijacked simultaneously by Tregs and Mφs (Pattern 6) after POD24 (Fig. 7B, C). However, more $CD8^+$T cells near FL cells were inhibited by Mφs but not Tregs (Pattern 7, 5 Fig. 7C,D). Taken together, these data suggest that Mφs not only serve an immunosuppressive function by themselves but also cooperate with Tregs more frequently to simultaneously inhibit cytotoxic T cells, to rationally yield enhanced immune-evading potentials of the TIME after POD24.

Discussion

In the current study, we used highly multiplexed IMC imaging of FL lymph node sections and constructed a spatially-resolved immunophenotypic map in FL with POD24 at a single-cell resolution level. The immune compositions in follicles and the interfollicular region significantly differed. FL cells with different phenotypes showed discrepancies in the fractions of neighboring immune cells. In addition, in the neighbors of FL cells in follicles, increased $CD163^-$Mφs with the upregulation of PD-1 ligands and decreased $CD8^+$T cells but with upregulated LAG3 were specifically found only at POD24. Further spatial interactions in tumor and immune cells demonstrated that FL cells interacted more frequently with immunosuppressive cells, especially Mφs, but less frequently with cytotoxic cells alone during POD24. Intriguingly, Tregs and Mφs evolved to collectively inhibit cytotoxic T cells in the follicles during POD24. Therefore, F -cells evolved to reside in a more immune-compromised microenvironment, escaping from immune attacks during POD24.

The current understanding of POD24 biology in FL is mainly based on alterations acquired at the onset of FL. These studies mostly focused on predicting POD24 at diagnosis, such as the gene-mutation-based prognostic model POD24-PI[3] and the TIME-based model BioFLIPI[19]. However, the lack of studies over the course of POD24 has hampered an understanding of its biology and therefore delayed new clinical trial designs. In a previous study, increased immune infiltration, including more Mφs and T cells at diagnosis, was negatively linked to POD24 incidence[7]; however, Mφ subsets varied significantly in the follicular and interfollicular regions. Canioni et al. showed that spatial distribution led to a different cut-off value to predict PFS and that the negative effect of Mφs on PFS was circumvented by rituximab in

cohorts of the GELA-GOELAMS FL-2000 trial[20]. However, when further identifying the Mφ subtype, $CD163^+$Mφs in the TIME showed a positive association with PFS owing to their capacity to mediate antibody-dependent cellular phagocytosis in rituximab-based immunochemotherapy[21]. However, these studies did not involve spatial information. Since most patients in our study received immunochemotherapy, both spatial distribution and subtypes were considered. Unexpectedly, the altered Mφ subset differed in the intra- and extra-follicular regions; $CD163^-$Mφs in follicles and $CD163^+$Mφs in the interfollicular regions significantly increased during POD24. These data suggested that $CD163^+$Mφs could be used predict the anti-lymphoma response to rituximab and that $CD163^-$Mφs in follicles also play a vital role in POD24. However, the underlying biological mechanisms need to be explored in the future.

IMC data on spatial location and cell phenotypes allowed us to accurately dissect the evolution of immune cells proximal to FL cells. Although classifying TAMs into M1- and M2-like types using CD163 and CD68 has been widely applied in many studies, accumulating evidence shows that the M1–M2 paradigm of TAMs cannot accurately reflect pro-tumor or anti-tumor functions[22]. Similarly, our study showed that the follicular $CD163^-$ TAMs and interfollicular $CD163^+$ TAMs surrounding FL cells significantly increased and displayed upregulated expression of PD-1 ligands during POD24. Interactions along the PD-L1/PD-1 axis could significantly impair T cell functions, indicating a negative effect of PD-$L1^+$Mφs on FL patients[23, 24]. Consistently, Blaker et al. showed that high degrees of intrafollicular PD-$L1^+$Mφs were associated with a shorter time to transformation in FL patients[25]. Further studies demonstrated that the IL-27/Stat3 axis induces the expression of PD-L1/2 on infiltrating Mφs in lymphoma, including FL[26]. However, anti-PD-1 monotherapy showed inferior efficacy, with only a 4% objective response rate in relapsed or refractory FL in the CheckMate 140 trial, which enrolled more than 45% POD24 patients[27]. Further biomarker analysis showed that more tumor-infiltrating $CD3^+PD\text{-}1^+$T cells and $CD68^+PD\text{-}L1^+$Mφs were observed in responders than in non-responders, but these differences were not statistically significant[27]. Nevertheless, it was remarkable that more TAMs but fewer $CD8^+$T cells around FL cells were observed in the TIME during POD24. Moreover, $CD8^+$T cells displayed the robust upregulation of LAG3. Yang et al. demonstrated that most LAG3 originates almost exclusively from the $PD\text{-}1^+$T-cell population, which was linked to T cell exhaustion[28]. The numbers of $CD3^+LAG\text{-}3^+$ or $TIM\text{-}3^+LAG\text{-}3^+$ cells were found to be correlated with poorer survival in FL patients[28]. These data could partially explain the poor efficacy of nivolumab. Therefore, the TIME evolved to be more suitable for the survival of FL cells under immune attacks, which was characterized by more TAMs with the upregulation of PD-1 ligands and fewer $CD8^+$T cells, but with an exhausted phenotype around FL cells.

Although a more immunosuppressive microenvironment was revealed by the frequency and phenotype of TAMs and $CD8^+$T cells neighboring tumor cells, interaction patterns in the TIME could provide more information to interpret its evolution during POD24. We found that more FL cells preferentially interacted with TAMs, rather than being directly exposed to cytotoxic T cells alone, after POD24. Despite the involvement of TAMs and Tregs in FL, the number of FL cells interacting with Tregs alone was not

significantly altered, indicating the critical role of TAMs during POD24. In addition to immune checkpoint engagement via the expression of PD-L1/2 as shown previously herein, TAMs can also directly inhibit $CD8^+$T responses by secreting inhibitory cytokines (such as IL-10), as well as the depletion of metabolites such as L-arginine and the production of reactive oxygen species[29]. Thus, the central role of TAMs might partially contribute to the disappointing response to anti-PD-1 therapy. However, as shown in other studies, rituximab could abrogate the negative effect of TAMs on the prognosis of FL in the chemotherapy era by activating TAMs and mediating antibody-dependent cellular phagocytosis effects[20]. Therefore, a regimen combining rituximab and anti-PD-1 therapy could show synergy in anti-FL effects. Consistently, anti-PD-L1 led to an unexpected ORR of 65% and a CR rate of 50% in patients with relapsed/refractory FL[30].

Notably, TAMs could also function indirectly by recruiting Tregs via CCL17/CCL22 and CCL20 or by inhibiting stimulatory populations such as dendritic cells[29]. We found that the dual protection of FL cells from immune attacks owing to Tregs and TAMs became more common during POD24. Moreover, more Tregs were co-localized with TAMs during POD24. Because FL cells did not secrete higher levels of Treg-specific chemokines, including CCL17 and CCL22, than normal B-cells[31], co-localization of Tregs and TAMs might be due to the recruitment of Tregs by TAMs. Essentially, the cooperation of Tregs and TAMs simultaneously led to the hijacking of more cytotoxic T cells in the follicles after POD24. Such cooperation between TAMs and Tregs might compromise the efficacy of combination rituximab and anti-PD-1 therapy. Therefore, combinatorial strategies involving drugs targeting Tregs, such as anti-CLTA-4 therapy[32], could be promising to improve clinical outcomes. However, biomarker-driven clinical trial studies are essential to determine the mechanisms underlying the co-localization of Mφs and Tregs during POD24.

In summary, IMC was used to develop a spatially preserved single-cell-resolution immunophenotypic atlas of FL and understand the evolution of the TIME during POD24, providing a novel and significant insight into TIME evolution during POD24. A more immunosuppressive TIME evolved during POD24, which was discovered and characterized based on the increased cooperation between TAMs and Tregs and the fewer $CD8^+$T cells but with higher expression of LAG3 around FL cells. Consequently, new therapeutic approaches harnessing LAG3, TAMs, and Tregs could improve clinical outcomes for patients with POD24.

Abbreviations

CR	Complete remission
FDCs	Follicular dendritic cells
FL	Follicular lymphoma
FRCs	Fibrotic reticular cells
ICOS	Inducible T-cell costimulator
IMC	Imaging mass cytometry
Mφs	macrophages
PD-1	Programmed cell death protein 1
PD-L1	Programmed cell death protein ligand 1
PD-L2	Programmed cell death protein ligand 2
POD24	Progression of disease with 24 months
ROIs	Regions of interest
SMA	Smooth muscle alpha actin
TAMs	Tumor associated macrophages
Tcons	Conventional CD4+T cells
Tfhs	Follicular helper T cells
TIM-3	T cell immunoglobulin and mucin domain 3
TIME	Tumor immune microenvironment
Tregs	Regulatory T cells

Declarations

Ethics approval and consent to participate

All samples were obtained after the patients provided informed consent. IRB approval for this study was granted by the Institutional Human Ethics Review Committee of the First Affiliated Hospital of Xiamen University and Sun Yat-sen University Cancer Center, in accordance with the Declaration of Helsinki

Availability of data and materials

The original contributions presented in the study are included in the article/supplementary materials. The IMC data will be uploaded in the public repository “Zenodo” once accepted. Further inquiries for data sharing can be directed to the corresponding authors during the review period.

Conflict of Interest

All authors declare that the research was conducted in the absence of any commercial or financial relationships that could be construed as a potential conflict of interest.

Funding: This work was financially supported by the National Natural Science Foundation of China (82170180 granted to Bing Xu, 81800163 granted to Jie Zha, 81800196 and 81770161 granted to Zhiming Li, 81900164 granted to Long Liu, 82100204 granted to Xingxing Yu), the Natural Science Foundation of Fujian Province (2020J011246 granted to Bing Xu), the Xiamen Municipal Bureau of Science and Technology (3502Z20209003 granted to Bing Xu, 3502Z20209008 granted for Zhifeng Li), and the Lymphoma Research Fund of the Chinese Anti-Cancer Association (CORP-117 granted to Bing Xu).

Author Contributions: L.L and XX. Y performed the experiments and data analysis. ZF. L, XH.H, J.Z, ZJ. L, Y.H, and ZM. L collected lymph node samples and clinical data; HJ. Z, Q.L, and X.J contributed to antibody tests and meta conjugating; L.L, XX.Y, KY. D, G.F, HF. Y, HY. Y, ZM. L, KH. Y, and B.X aided in interpreting the results and worked on the manuscript; L.L and B.X conceived and planned the experiments. All authors have given approval to the final version of the manuscript.

Acknowledgments

The authors thank the department of pathology of the first affiliated hospital of Xiamen university for their assistance in choosing ROIs.

References

1. Lackraj T, Goswami R, Kridel R. Pathogenesis of follicular lymphoma. Best practice & research Clinical haematology. 2018;31(1):2–14.
2. Carbone A, Roulland S, Gloghini A, Younes A, von Keudell G, Lopez-Guillermo A, et al. Follicular lymphoma. Nat Rev Dis Primers. 2019;5(1):83.
3. Jurinovic V, Kridel R, Staiger AM, Szczepanowski M, Horn H, Dreyling MH, et al. Clinicogenetic risk models predict early progression of follicular lymphoma after first-line immunochemotherapy. Blood. 2016;128(8):1112–20.
4. Sugimoto T, Watanabe T. Follicular Lymphoma: The Role of the Tumor Microenvironment in Prognosis. Journal of clinical and experimental hematopathology: JCEH. 2016;56(1):1–19.
5. Huet S, Sujobert P, Salles G. From genetics to the clinic: a translational perspective on follicular lymphoma. Nat Rev Cancer. 2018;18(4):224–39.
6. Wahlin BE, Sander B, Christensson B, Ostenstad B, Holte H, Brown PD, et al. Entourage: the immune microenvironment following follicular lymphoma. Blood cancer journal. 2012;2(1):e52.
7. Tobin JWD, Keane C, Gunawardana J, Mollee P, Birch S, Hoang T, et al. Progression of Disease Within 24 Months in Follicular Lymphoma Is Associated With Reduced Intratumoral Immune Infiltration.

Journal of clinical oncology: official journal of the American Society of Clinical Oncology. 2019;37(34):3300–9.

8. Ame-Thomas P, Tarte K. The yin and the yang of follicular lymphoma cell niches: role of microenvironment heterogeneity and plasticity. Seminars in cancer biology. 2014;24:23–32.
9. Pantanowitz L, Preffer F, Wilbur DC. Advanced imaging technology applications in cytology. Diagnostic cytopathology. 2018.
10. Rawlins CM, Salisbury JP, Feldman DR, Isim S, Agar NY, Luther E, et al. Imaging and Mapping of Tissue Constituents at the Single-Cell Level Using MALDI MSI and Quantitative Laser Scanning Cytometry. Methods in molecular biology (Clifton, NJ). 2015;1346:133 – 49.
11. Chang Q, Ornatsky OI, Siddiqui I, Loboda A, Baranov VI, Hedley DW. Imaging Mass Cytometry. Cytometry Part A: the journal of the International Society for Analytical Cytology. 2017;91(2):160–9.
12. Keren L, Bosse M, Marquez D, Angoshtari R, Jain S, Varma S, et al. A Structured Tumor-Immune Microenvironment in Triple Negative Breast Cancer Revealed by Multiplexed Ion Beam Imaging. Cell. 2018;174(6):1373-87.e19.
13. Schulz D, Zanotelli VRT, Fischer JR, Schapiro D, Engler S, Lun XK, et al. Simultaneous Multiplexed Imaging of mRNA and Proteins with Subcellular Resolution in Breast Cancer Tissue Samples by Mass Cytometry. Cell Syst. 2018;6(1):25–36 e5.
14. Giesen C, Wang HA, Schapiro D, Zivanovic N, Jacobs A, Hattendorf B, et al. Highly multiplexed imaging of tumor tissues with subcellular resolution by mass cytometry. Nat Methods. 2014;11(4):417–22.
15. Ijsselsteijn ME, van der Breggen R, Farina Sarasqueta A, Koning F, de Miranda N. A 40-Marker Panel for High Dimensional Characterization of Cancer Immune Microenvironments by Imaging Mass Cytometry. Frontiers in immunology. 2019;10:2534.
16. Han G, Spitzer MH, Bendall SC, Fantl WJ, Nolan GP. Metal-isotope-tagged monoclonal antibodies for high-dimensional mass cytometry. Nat Protoc. 2018;13(10):2121–48.
17. Schapiro D, Jackson HW, Raghuraman S, Fischer JR, Zanotelli VRT, Schulz D, et al. histoCAT: analysis of cell phenotypes and interactions in multiplex image cytometry data. Nat Methods. 2017;14(9):873–6.
18. Levine JH, Simonds EF, Bendall SC, Davis KL, Amir el AD, Tadmor MD, et al. Data-Driven Phenotypic Dissection of AML Reveals Progenitor-like Cells that Correlate with Prognosis. Cell. 2015;162(1):184–97.
19. Mondello P, Fama A, Larson MC, Feldman AL, Villasboas JC, Yang ZZ, et al. Lack of intrafollicular memory CD4 + T cells is predictive of early clinical failure in newly diagnosed follicular lymphoma. Blood cancer journal. 2021;11(7):130.
20. Canioni D, Salles G, Mounier N, Brousse N, Keuppens M, Morchhauser F, et al. High numbers of tumor-associated macrophages have an adverse prognostic value that can be circumvented by rituximab in patients with follicular lymphoma enrolled onto the GELA-GOELAMS FL-2000 trial.

Journal of clinical oncology: official journal of the American Society of Clinical Oncology. 2008;26(3):440–6.

21. Kridel R, Xerri L, Gelas-Dore B, Tan K, Feugier P, Vawda A, et al. The Prognostic Impact of CD163-Positive Macrophages in Follicular Lymphoma: A Study from the BC Cancer Agency and the Lymphoma Study Association. Clinical cancer research: an official journal of the American Association for Cancer Research. 2015;21(15):3428–35.
22. Wu K, Lin K, Li X, Yuan X, Xu P, Ni P, et al. Redefining Tumor-Associated Macrophage Subpopulations and Functions in the Tumor Microenvironment. Frontiers in immunology. 2020;11:1731.
23. Yang ZZ, Grote DM, Ziesmer SC, Xiu B, Novak AJ, Ansell SM. PD-1 expression defines two distinct T-cell sub-populations in follicular lymphoma that differentially impact patient survival. Blood cancer journal. 2015;5:e281.
24. Myklebust JH, Irish JM, Brody J, Czerwinski DK, Houot R, Kohrt HE, et al. High PD-1 expression and suppressed cytokine signaling distinguish T cells infiltrating follicular lymphoma tumors from peripheral T cells. Blood. 2013;121(8):1367–76.
25. Blaker YN, Spetalen S, Brodtkorb M, Lingjaerde OC, Beiske K, Ostenstad B, et al. The tumour microenvironment influences survival and time to transformation in follicular lymphoma in the rituximab era. British journal of haematology. 2016;175(1):102–14.
26. Horlad H, Ma C, Yano H, Pan C, Ohnishi K, Fujiwara Y, et al. An IL-27/Stat3 axis induces expression of programmed cell death 1 ligands (PD-L1/2) on infiltrating macrophages in lymphoma. Cancer Sci. 2016;107(11):1696–704.
27. Armand P, Janssens A, Gritti G, Radford J, Timmerman J, Pinto A, et al. Efficacy and safety results from CheckMate 140, a phase 2 study of nivolumab for relapsed/refractory follicular lymphoma. Blood. 2021;137(5):637–45.
28. Yang ZZ, Kim HJ, Villasboas JC, Chen YP, Price-Troska T, Jalali S, et al. Expression of LAG-3 defines exhaustion of intratumoral PD-1(+) T cells and correlates with poor outcome in follicular lymphoma. Oncotarget. 2017;8(37):61425–39.
29. DeNardo DG, Ruffell B. Macrophages as regulators of tumour immunity and immunotherapy. Nature reviews Immunology. 2019;19(6):369–82.
30. Nastoupil LJ, Westin JR, Fowler NH, Fanale MA, Samaniego F, Oki Y, et al. Response rates with pembrolizumab in combination with rituximab in patients with relapsed follicular lymphoma: Interim results of an on open-label, phase II study. Journal of Clinical Oncology. 2017;35(15_suppl):7519-.
31. Ai WZ, Hou JZ, Zeiser R, Czerwinski D, Negrin RS, Levy R. Follicular lymphoma B cells induce the conversion of conventional CD4 + T cells to T-regulatory cells. International journal of cancer. 2009;124(1):239–44.
32. Winograd R, Byrne KT, Evans RA, Odorizzi PM, Meyer AR, Bajor DL, et al. Induction of T-cell Immunity Overcomes Complete Resistance to PD-1 and CTLA-4 Blockade and Improves Survival in Pancreatic Carcinoma. Cancer immunology research. 2015;3(4):399–411.

Figures

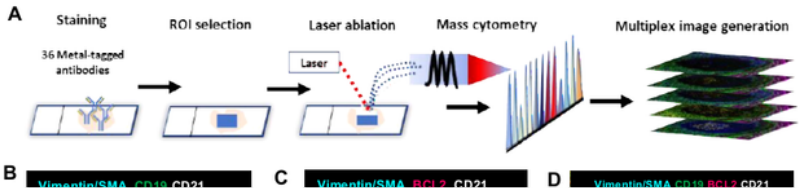

Figure 1

Imaging mass cytometry (IMC) workflow and illustration of measurement

(A), A laser ablates the tissue spot-by-spot, generating clouds of atomized and ionized particles in inductively coupled plasma before analysis by mass cytometry. Based on ion cloud compositions, an image of the ablated area is created for each measured marker. (B–D), Follicular lymphoma (FL) cells in the follicles expressed CD19 (B) and Bcl-2 (C), and the overlay of Bcl-2 and CD19 is shown (D). (E–H), Immune compositions such as $CD4^{+}$T (E) and $CD8^{+}$T cells (F) and macrophages (H) were well presented by IMC. (I), The lymph node structure shows that areas between the follicular and interfollicular boundaries were clearly displayed with SMA, vimentin, and CD21. (J), IMC images were segmented into cells. (K), Imaged cells were classified into cell types. Cells were first divided into 12 categories. (L), Quantitative biomarker expression of a specific cluster could be measured. (M), By retrieving spatial data, neighborhood information (center) was used to systematically analyze cell–cell interactions.

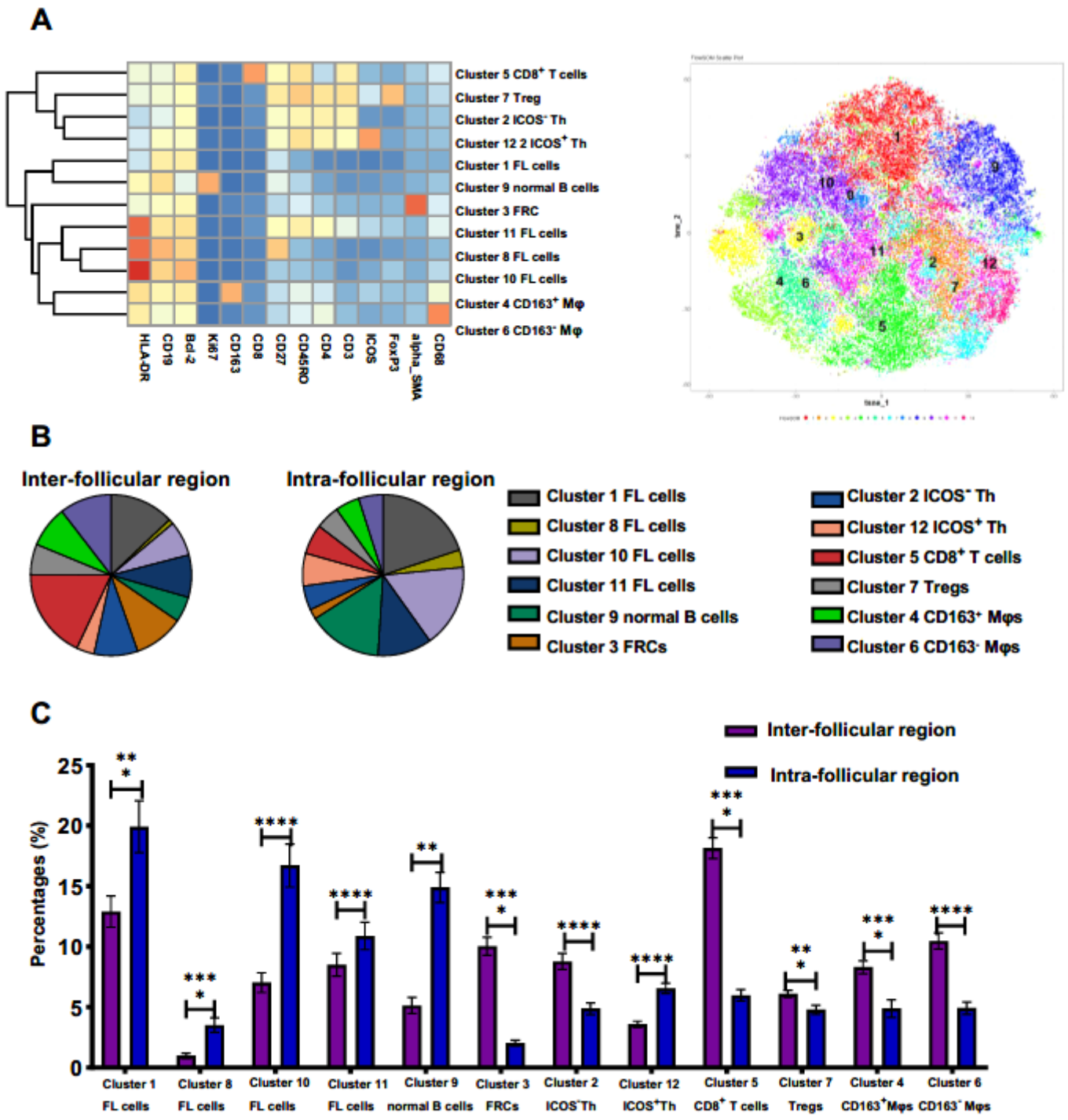

Figure 2

The landscape of tumor immune microenvironment (TIME) in follicular lymphoma (FL)

(A), Cells were first divided into 12 categories according to the indicated markers displayed by the heatmap (left) and t-SNE (right). (B–C), Heterogeneity in follicular and interfollicular regions is presented in pie charts (B); comparisons were performed (C).

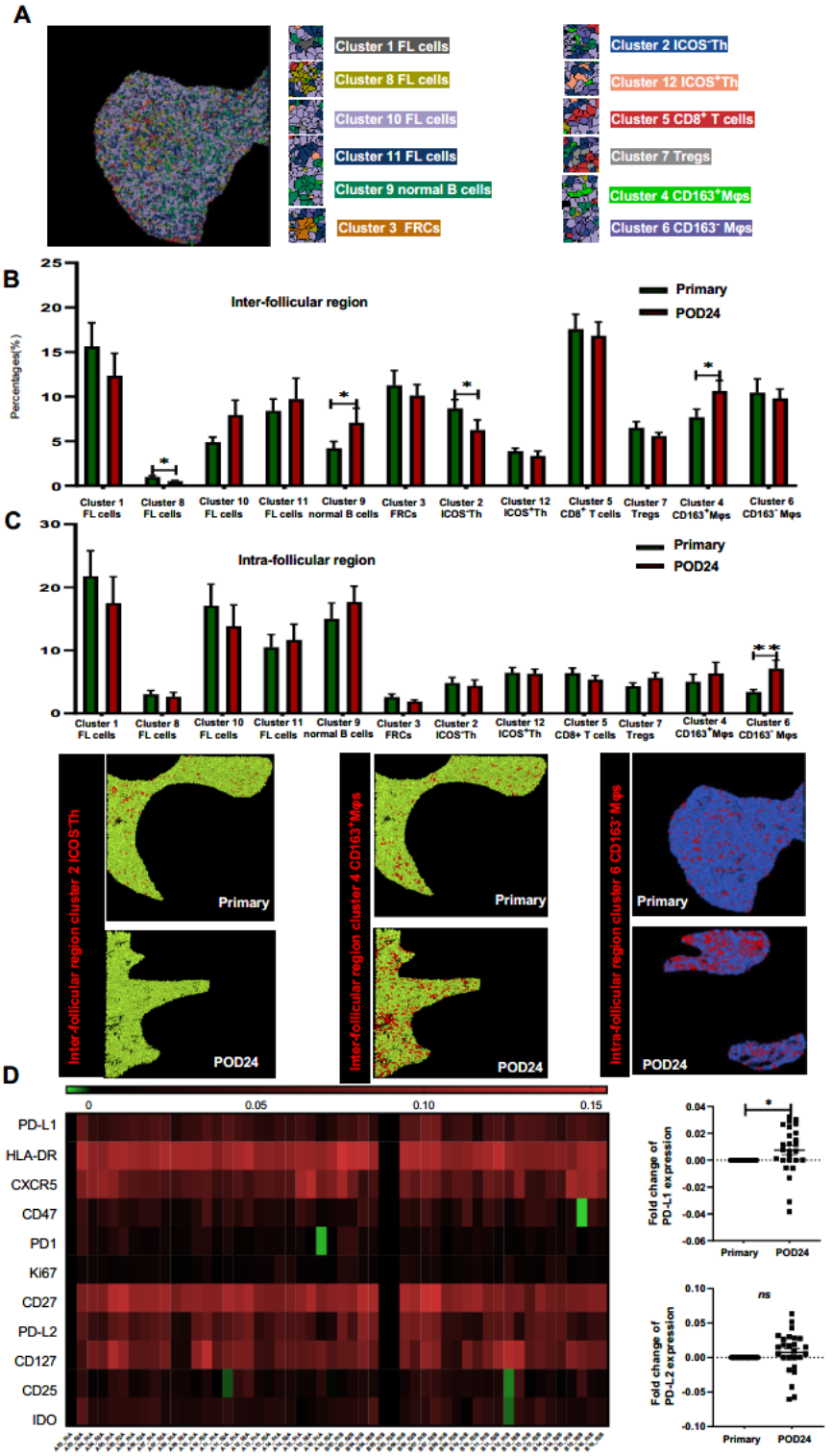

Figure 3

Dynamic alterations in cell compositions in follicular and interfollicular regions during progression of disease within 24 months (POD24) in follicular lymphoma (FL)

(A), The cell compositions, including the 12 clusters in the total area of FL. (B–C), Cell composition evolution in the interfollicular (B) and follicular regions (C) during POD24 in FL. (D), Phenotypic

alterations in cluster 8 FL cells during POD24.

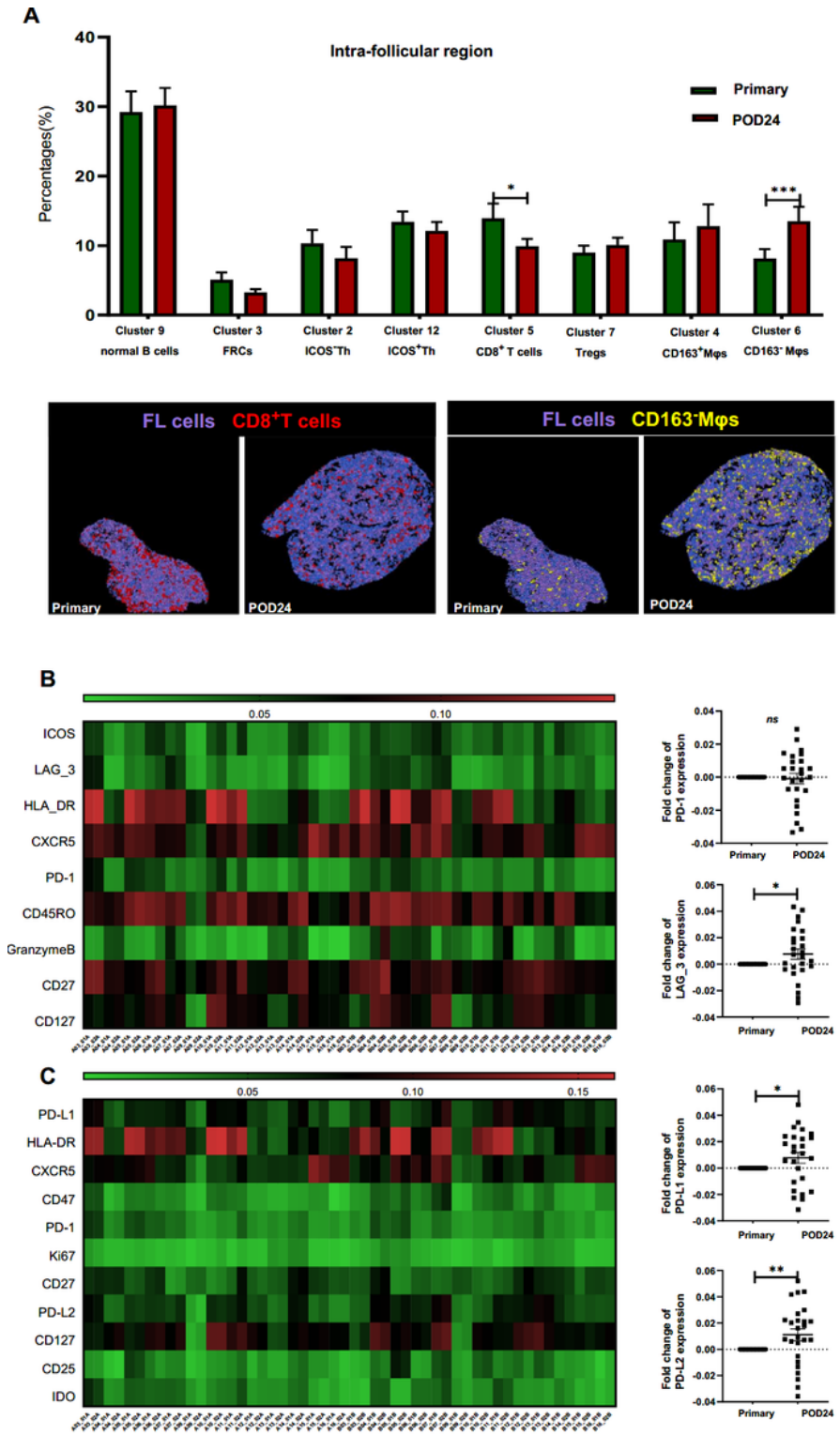

Figure 4

The evolution of immune components around follicular lymphoma (FL)cells in the follicles during progression of disease within 24 months (POD24) in FL

(A), Alterations in the frequency of immune cells surrounding FL cells during POD24. (B), Heatmap of phenotypic alterations (left), and PD-1 and LAG-3 expression (right) in $CD8^+$T cells during POD24 in FL. (C), Heatmap of phenotypic alterations (left), and PD-L1/2 expression (right) in $CD163^-$ macrophages during POD24 in FL.

Figure 5

Evolution of follicular lymphoma (FL) and immune cell interactions during progression of disease within 24 months (POD24) in FL

(A), Scheme of analysis of interactions between FL and three types of immune cells. In total, eight interaction patterns are listed in the table (right) according to the co-location of FL and immune cells. The fractions of FL cells with different interactions accounting for total FL cells were calculated. Significant decrease in FL cells interacting with $CD8^+$T cells alone as shown in Pattern 2 (B) after POD24; higher percentages of FL cells interacted alone as shown in pattern 4 (C) and simultaneously with macrophages (Mφs) and regulatory T cells (Tregs) as shown in Pattern 7 (D) in the follicles during POD24 in FL. Additionally, in the interfollicular regions, decreased FL cells interacted with $CD8^+$T cells alone as shown in pattern 2 (E), whereas more FL cells interacted with Mφs alone as shown in Pattern 4 (F) during POD24 in FL.

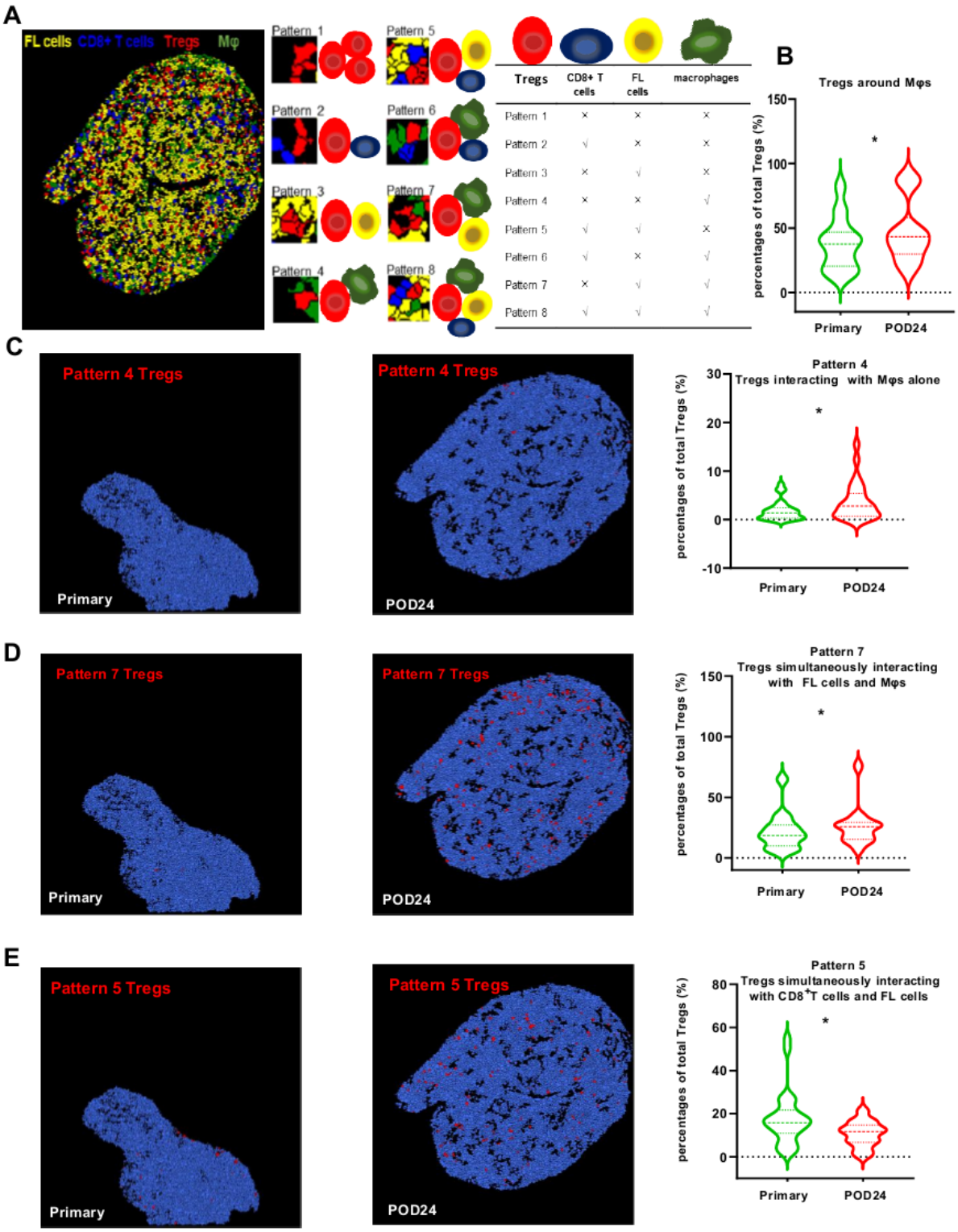

Figure 6

Evolution of cell interactions of regulatory T cells (Tregs) during progression of disease within 24 months (POD24) in follicular lymphoma (FL)

(A), Scheme of analysis of interactions between Tregs and two types of immune and FL cells. In total, eight interaction patterns are listed in the table (right) according to the co-location of Tregs and three

other cell types. The fractions of Tregs with different interactions accounting for total Tregs were calculated. (B), The fractions of Tregs around macrophages (Mφs) were significantly larger after POD24. Further spatial interactions showed that larger fractions of Tregs not only interacted with Mφs alone as shown in Pattern 4 (C) but also interacted with simultaneously Mφs and FL cells as shown in Pattern 7 (D) during POD24 in FL. However, fewer Tregs interacted with FL cells alone as shown in Pattern 5 (E) in the follicles during POD24 in FL.

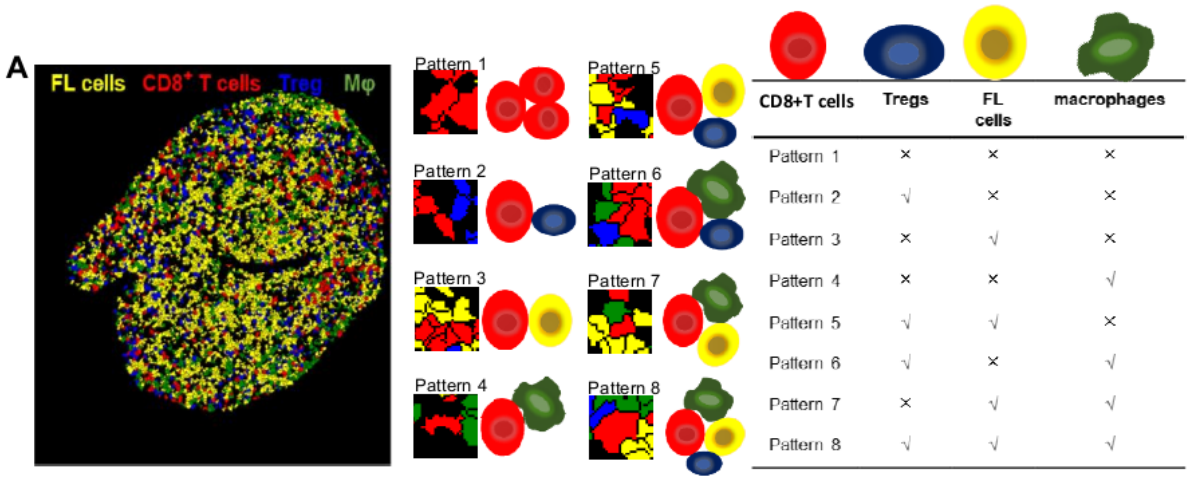

CD8+T cells	Tregs	FL cells	macrophages
Pattern 1	×	×	×
Pattern 2	√	×	×
Pattern 3	×	√	×
Pattern 4	×	×	√
Pattern 5	√	√	×
Pattern 6	√	×	√
Pattern 7	×	√	√
Pattern 8	√	√	√

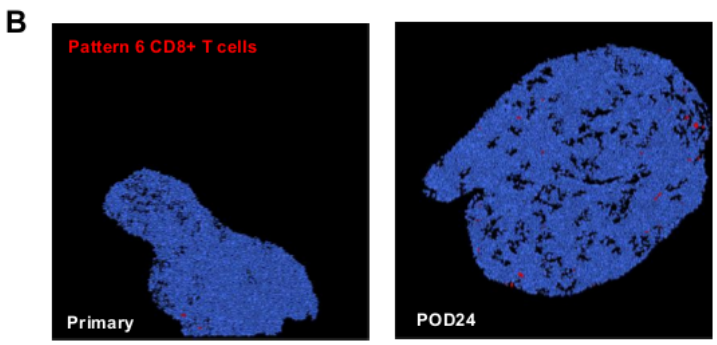

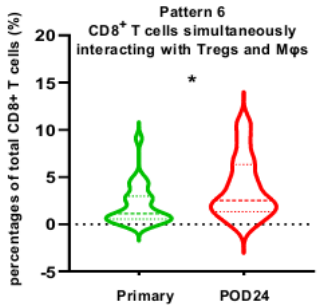

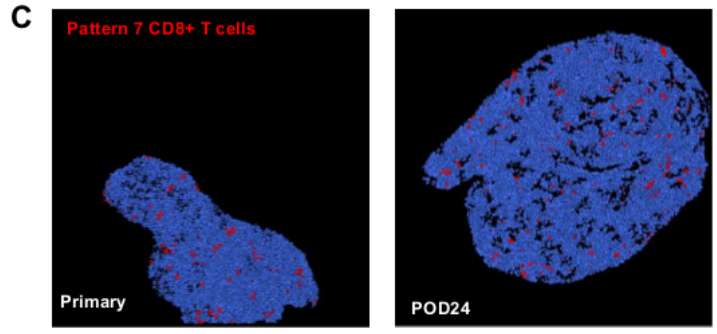

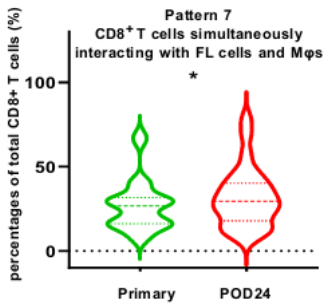

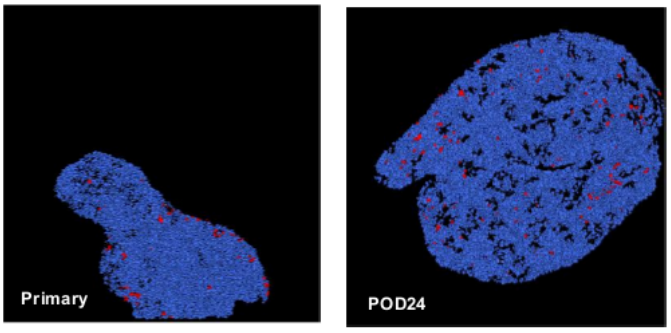

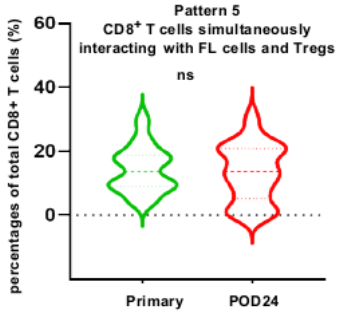

Figure 7

Evolution of cell interactions with $CD8^+$T cells during progression of disease within 24 months (POD24) in follicular lymphoma (FL)

(A), Scheme of analysis of interactions between $CD8^+$T cells and two types of immune cells and FL cells. In total, eight interaction patterns are outlined in the table (right) according to the co-localization of $CD8^+$ T cells and three other cell types. The fractions of $CD8^+$ T cells with different interactions accounting for total $CD8^+$ T cells were calculated. More $CD8^+$ T cells were inhibited simultaneously by regulatory T cells (Tregs) and macrophages (Mφs) as shown in Pattern 6 (B) during POD24 in FL. In addition, more $CD8^+$ T cells interacted with Mφs, rather than Tregs alone, as shown in Pattern 7 (C) and Pattern 5(D) during POD24 in FL.

Supplementary Files

This is a list of supplementary files associated with this preprint. Click to download.

- Table1.xlsx
- Supplementarytable2.xlsx